

Control of complex quantum structures in droplet epitaxy

J. M. A. Chawner¹, Y. Chang¹, P. D. Hodgson¹, M. Hayne¹, A. J. Robson¹, A. M. Sanchez², Q. Zhuang¹

¹Department of Physics, Lancaster University, Lancaster, LA1 4YB, UK.

²Department of Physics, Warwick University, Coventry, CV4 7AL, UK.

E-mail: j.chawner@lancaster.ac.uk

June 2019

Abstract. We report the controllable growth of GaAs quantum complexes in droplet molecular-beam epitaxy, and the optical properties of self-assembled $\text{Al}_x\text{Ga}_{1-x}\text{As}$ quantum rings embedded in a superlattice. We found that Ga droplets on a GaAs substrate can retain their geometry up to a maximum temperature of 490 °C during post-growth annealing, with an optimal temperature of 320 °C for creating uniform and symmetric droplets. Through controlling only the crystallisation temperature under As_4 in the range of 450 °C to 580 °C, we can reliably control diffusion, adsorption and etching rates to produce various GaAs quantum complexes such as quantum dots, dot pairs and nanoholes. $\text{Al}_x\text{Ga}_{1-x}\text{As}$ quantum rings are also realised within these temperatures via the adjustment of As beam equivalent pressure. We found that crystallisation using As_2 molecules in the place of As_4 creates smaller diameter quantum rings at higher density. The photoluminescence of As_2 grown $\text{Al}_x\text{Ga}_{1-x}\text{As}$ quantum rings embedded in a superlattice shows a dominant emission from the quantum rings at elevated temperatures. This observation reveals the properties of the quantum ring carrier confinement and their potential application as efficient photon emitters.

Keywords: Droplet Epitaxy, Molecular Beam Epitaxy, Quantum Structure, Photoluminescence, Atomic Force Microscopy, Transmission Electron Microscopy.

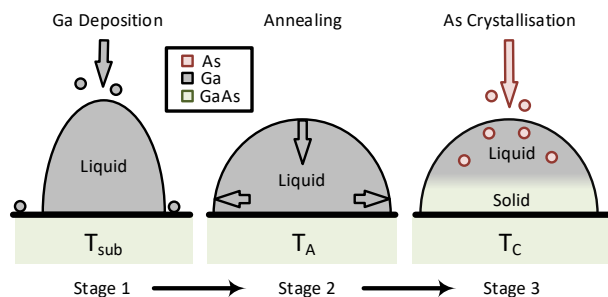


Figure 1. The three stages of droplet epitaxy growth. Stage 1: A few atomic monolayers of a group III element (*e.g.* Ga) is deposited. These nucleate into droplets, balancing the surface free energy at the droplet/vacuum/surface interface. Stage 2: The substrate is heated to anneal the droplets. This affects the droplets dimensions due to a change in contact angle. Stage 3: A group V element (*e.g.* As) is deposited. This combines with the Ga rich droplets at the liquid/solid interface to create crystallised GaAs. This is done until the liquid material is entirely crystallised.

1. Introduction

Quantum dots (QDs) are nano-scale, zero-dimensional structures that confine charge carriers into quantised energy levels; a property which has extensive applications within optoelectronics and quantum computing [1, 2, 3]. A discrete energy system is observed within an atom's density of states, but whereas atoms have energy levels fixed by nature, the energy structure of QDs are directly related to their shape, material composition and strain. A successful approach for the fabrication of QDs is self-assembled growth by molecular beam epitaxy (MBE) or metal-organic chemical vapour deposition using the Stranski-Krastanov technique (S-K), a layer-plus-island growth mode generated from lattice strain [4]. In S-K growth, particular material combinations need to be used, with a lattice mismatch of a few percent, limiting the options available. Dislocations can occur as a consequence of lattice strain [5].

One alternative to S-K growth is droplet epitaxy (DE), which creates QDs from consecutive depositions of group III and V materials (Figure 1). DE can be a strain-free growth method, which helps reduce the likelihood and severity of defects and is therefore advantageous for optoelectronic devices [6]. In addition, the growth mechanism can be performed with a wider range of material combinations and substrate orientations than S-K growth, including those that are lattice-matched as well as lattice-mismatched [7]. Due to the consecutive nature of DE, each stage of epitaxy can be adjusted as desired. For example, it has been shown that the substrate annealing temperature at each stage of DE affects the resulting nanostructure architecture [8], with many different types of structures

realised via DE [9, 10, 11, 12], including nanowires [13].

This paper aims to explore the DE procedure to allow controlled and efficient production of specific quantum structures with high optical efficiency. For the device materials, GaAs and $\text{Al}_x\text{Ga}_{1-x}\text{As}$ were chosen due to their type-I heterojunction properties, which are capable of fabricating optoelectronic single-photon devices operating in the near-infrared band. Furthermore, the similarity in lattice constant between the two materials produces little to no strain, making GaAs/ $\text{Al}_x\text{Ga}_{1-x}\text{As}$ QDs inaccessible to the widely exploited S-K mode, and thus substantially less investigated than InAs/GaAs QDs, for example. QD's have been previously fabricated with these materials on a (111) surface to produce quantum entangled photons [14], a testament to the materials defect-free properties and optoelectronic abilities. They were also recently used to clearly demonstrate the existence of the somewhat elusive phonon bottleneck [15], while the lack of strain and considerable knowledge of the GaAs/ $\text{Al}_x\text{Ga}_{1-x}\text{As}$ system makes modelling of their properties relatively straight forward [16]. First, the effect of annealing temperature on metal Ga droplets is investigated on a GaAs substrate. Then we explore the effect of substrate temperature on the evolution of self-assembled GaAs nanostructures during As exposure for crystallisation. Various quantum complexes were obtained from the same recipe, with only the crystallisation temperature as a variable. A comparison of the effects of using molecules of As_2 or As_4 for crystallisation on an $\text{Al}_x\text{Ga}_{1-x}\text{As}$ matrix was investigated. Using As_2 simplifies the MBE growth procedure as no growth pause is needed to turn down the high cracker temperature, as would be the case for using As_4 . Finally, a sample of GaAs quantum rings (QRs) grown with optimal conditions and embedded in an AlAs/GaAs superlattice (SL), was fabricated. Photoluminescence (PL) studies of this sample reveal good zero-dimensional carrier confinement, indicating its potential application as a single photon emitter.

2. Experimental Details

The samples were grown in a conventional MBE reactor equipped with effusion cells for group III elements and a valved cracker for As_4 or As_2 molecules. A GaAs (001) substrate was heated to 580°C and a 200 nm-thick GaAs buffer layer was grown. Then the substrate temperature was reduced to 250°C with the As cracker temperature set to 650°C . The valve and shutter were closed for 30 minutes to optimise the background vacuum environment to $\approx 10^{-10}$ torr. Next, the droplet growth was performed by depositing 3 monolayers (MLs) of Ga at a growth rate of

Sample	Growth Surface	T_A	T_C	BEP	h (nm)	d (nm)	Density (cm^{-2})	Structure
A	GaAs	320	-	-	8.0 ± 0.2	80 ± 3	$(5.1 \pm 0.2) \times 10^9$	Droplet
B	GaAs	490	-	-	5.5 ± 0.5	100 ± 10	$(4.9 \pm 0.2) \times 10^9$	Droplet
C	GaAs	580	-	-	-	-	-	Lumpy
D	GaAs	320	450	10^{-5}	8.3 ± 0.5	90 ± 10	$(4.9 \pm 0.2) \times 10^9$	QD
E	GaAs	320	520	10^{-5}	6 ± 1	120 ± 10	$(5.0 \pm 0.2) \times 10^9$	QD pair
F	GaAs	320	580	10^{-5}	-9.0 ± 0.5	100 ± 10	$(5.2 \pm 0.2) \times 10^9$	Nanohole
G	$\text{Al}_{0.32}\text{Ga}_{0.68}\text{As}$	320	520	10^{-6}	1.5 ± 0.5	40 ± 10	$(1.9 \pm 0.1) \times 10^{10}$	QR
H	$\text{Al}_{0.32}\text{Ga}_{0.68}\text{As}$	320	520	10^{-6}	0.9 ± 0.1	35 ± 10	$(3.7 \pm 0.1) \times 10^{10}$	QR (As_2)
I	GaAs	320	520	10^{-6}	10 ± 1	110 ± 10	$(3.0 \pm 0.1) \times 10^8$	QR (As_2)

Table 1. A direct comparison of samples A-I studied here. T_A and T_C represent the substrate temperature during annealing and crystallisation respectively. BEP represents the beam equivalent pressure of As flux during the 10 min crystallisation. h and d represent the height and diameter of the final nanostructures respectively. Samples D-G were crystallised with As_4 , while samples H and I were crystallised with As_2 . All samples were created with 3 MLs of Ga, except sample I which used 1 ML.

0.5 ML s^{-1} for 6 seconds at a substrate temperature of 250°C (Figure 1, stage 1). The sample was split *ex situ* into three separate segments and returned to the MBE vacuum storage. During this procedure the samples were stored under nitrogen for no more than 30 mins, to reduce oxidation. Each sample was then subjected to different annealing temperatures for 20 mins; 320°C , 490°C and 580°C for samples A, B and C respectively in Table 1. All annealing temperatures were ramped to at a rate between $10^\circ\text{C}/\text{min}$ and $40^\circ\text{C}/\text{min}$ to maintain a constant ramp time between samples.

A new batch of Ga droplets were annealed at 320°C (recipe of sample A) and were then split *ex situ* into 3 samples; D, E, F, before being returned to the MBE chamber individually. The samples were subjected to 10 mins of As_4 irradiation with a beam equivalent pressure (BEP) of 10^{-5} torr, each at a different substrate temperature throughout crystallisation, *i.e.*, 450°C , 520°C and 580°C for samples D, E and F respectively in Table 1. All crystallisation temperatures were ramped to at a rate between $10^\circ\text{C}/\text{min}$ and $40^\circ\text{C}/\text{min}$ to maintain a constant ramp time between samples. This was also done for all crystallisation temperature mentioned in future samples.

In order to investigate As_2 as compared with As_4 crystallisation, the recipe for sample E was again reproduced to create two new samples. However, before the Ga droplet deposition, a 50 nm $\text{Al}_{0.32}\text{Ga}_{0.68}\text{As}$ layer was grown on the GaAs (001) substrate to create a type-I nanostructure/surface heterojunction for optoelectronic functionality. The BEP was also reduced to 10^{-6} torr, which has been shown to encourage QR growth [17]. QR's were chosen for their good characteristics as photonic sources [18]. Each sample remained in the MBE chamber and was crystallised at 520°C with a 10^{-6} torr BEP, one under As_4 and the other under As_2 (samples G and H respectively in Table 1).

Finally, a sample of As_2 -crystallised QRs embed-

ded in a SL (sample I in Table 1) was fabricated to study the optical properties of the QRs created by As_2 . Droplet growth was initiated on a GaAs (001) substrate with a 420 nm thick GaAs/AlAs (2.8 nm/2.8 nm) SL structure. A 50-nm-thick $\text{Al}_{0.32}\text{Ga}_{0.68}\text{As}$ layer was then grown before QRs were fabricated with the almost identical recipe to sample H, but with a reduced liquid Ga volume of 1 ML, to limit the areal density of structures. This was originally done in an attempt to allow optical studies on a single QR, however the areal density was still too high to perform such a measurement, so the sample was tested as a whole. The GaAs QRs were capped by another 50-nm-thick layer of $\text{Al}_{0.32}\text{Ga}_{0.68}\text{As}$, followed by another SL, to form a potential well to trap carriers locally in the QRs during optical stimulation. Then finally another set of QR's were fabricated on the surface for topographic observations. A cross section of a QR within sample I was observed via transmission electron microscopy (TEM). X-ray diffraction measurements of the sample were taken to analyse the structural details of the SL and the Al/Ga balance. The optical properties were studied by PL measurements with a 532-nm laser for a temperature range of 4 K to 100 K in an Oxford Instruments flow cryostat. The morphology of all the quantum complexes was investigated with atomic force microscopy (AFM) on a Multimode 8 system.

3. Results and Discussion

In this discussion, surface processes during fabrication are approximately modelled to first order using the Arrhenius equation, which relates an event x occurrence rate R_x with surface location \vec{r} and temperature T [19]:

$$R_x(\vec{r}, T) = v_x e^{-E_x(\vec{r})/k_B T}, \quad (1)$$

where v_x typically represents an intrinsic frequency for the process, such as atomic vibration. E_x is the

activation energy for the event x at position \vec{r} and k_B is the Boltzmann constant. This model has been used as the core principle in droplet epitaxy Monte Carlo simulations which have accurately recreated experimental observation [17, 20]. Each process rate is limited by intrinsic frequency v_x . When $k_B T \gtrsim \bar{E}_x$, the process rate becomes a significant fraction of the limiting frequency v_x , where \bar{E}_x is the average activation energy over the surface defined by \vec{r} . Therefore, the processes may switch in dominance as temperature changes, dependent on v_x .

3.1. Annealing effect on Ga droplets

Figure 2 shows the AFM images of the Ga droplets annealed (Figure 1, stage 2) at temperatures of 320 °C, 490 °C and 580 °C for samples A, B and C respectively. It is evident that annealing has a significant effect on the geometry of the Ga droplets. Low annealing temperature (sample A) yielded droplets with a diameter of 80 ± 3 nm, height of 8.0 ± 0.2 nm and an areal structure density of $(5.1 \pm 0.2) \times 10^9 \text{ cm}^{-2}$. A higher annealing temperature 490 °C (sample B) led to droplets with a diameter of 100 ± 10 nm, height of 5.5 ± 0.5 nm and a similar areal density of $(4.9 \pm 0.2) \times 10^9 \text{ cm}^{-2}$. Above this temperature a lumpy surface was produced without individual nanostructures (sample C at 580 °C). Assuming that the droplet/surface GaAs interface energy is lowered with higher temperature, the larger droplet diameter at 490 °C (sample B) can be attributed to a reduced droplet contact angle and higher degree of surface wetting caused by the equilibrium of surface energy at the droplet/surface/vacuum interface [4]. Raising the temperature to 580 °C (sample C) demonstrates a more complete wetting of the surface, and therefore a loss of distinguishable nanostructures.

3.2. Crystallisation under As exposure

An investigation was made into the effect of substrate temperature during As_4 crystallisation (Figure 1, stage 3) on final nanostructure geometry. The AFM scans in Figure 3 clearly show the capability of varying crystallisation temperature to introduce different forms of nanostructure, the dimensions of which are given in Table 1. Under As flux, many competing processes determine the movement and settling location of As adatoms, all of which can be modelled to first order via the Arrhenius equation (Equation 1). In the temperature range explored here, the main driving first order processes observed within the Ga droplets are diffusion, adsorption and etching of Ga and As liquid material. The intrinsic frequency for all the processes are dependent on many factors, including the Debye frequency of the substrate for surface processes and

the surrounding density of Ga and As for all processes [20]. This creates variance in process rates between different adatoms.

At 450 °C (sample D), single QDs were formed with a diameter of 90 ± 10 nm and height of 8.3 ± 0.5 nm. This indicates that Ga and As surface adsorption rates R_A are now active and dominant, allowing a complete and even crystallisation of the Ga droplet at the liquid/solid interface without diffusion or etching effects impacting the structure significantly.

Further increase of the temperature to 520 °C (sample E) formed QD pairs with a total structure diameter of 120 ± 10 nm in the $[1\bar{1}0]$ axis and height of 6 ± 1 nm. The orientation of the QD pairs demonstrate the anisotropic surface diffusion taking place. At this temperature, the As diffusion rate R_D within the Ga droplet is more active, allowing the As adatoms to crystallise at the energetically favourable liquid/solid/vacuum triple point quicker than the liquid/solid interface. Without surface tension, the droplet collapses into itself, forcing material away from the centre. The potential energy surface of GaAs(001) attracts the liquid material anisotropically in the $[1\bar{1}0]$ and $[\bar{1}10]$ directions [21, 22, 23]. This effect results in the crystallisation of two separate QDs that form opposite the original droplet centre.

At a substrate temperature of 580 °C (sample F), the liquid material forms nanoholes within the GaAs substrate with a diameter of 100 ± 10 nm and depth of 9.0 ± 0.5 nm. As observed previously [24], deposited As_4 that comes into contact with the droplet diffuses outward from the centre and crystallises at the liquid/solid/vacuum interface faster than any other location (also observed in sample E). At this higher temperature, As dissolution into the Ga droplet is now fully activated and the etching rate R_E has become the dominant process. The Ga droplet significantly etches the GaAs substrate at the liquid/solid interface, causing the liquid material to drill downwards. Liberated surface Ga and As supplement the liquid material and the As atoms diffuse through to crystallise at the liquid/solid/vacuum triple point.

These growth observations show that GaAs DE growth can create topographies with quantum artefacts at temperatures up to 580 °C on an GaAs substrate. For the liquid material, R_A has observable dominance up to 520 °C, R_D has noticeable impact at 520 °C and R_E has dominance at 580 °C. The order of process dominance with increasing temperature, *i.e.* adsorption, diffusion, etching, agree with the activation energies for an As atom on the solid/liquid interface: \bar{E}_A , \bar{E}_D , $\bar{E}_E = 0.5 \text{ eV}$, 0.7 eV , 0.9 eV respectively [17]. However, the temperatures we report differ from previous findings which show dot-like growth occurs up to 250 °C and ring-like growth occurs at around

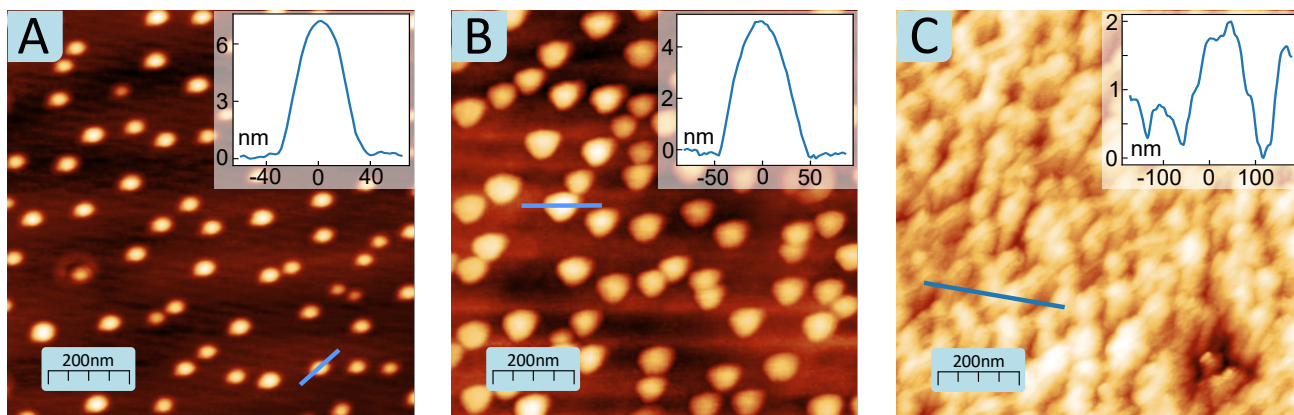


Figure 2. $1 \times 1 \mu\text{m}^2$ AFM images and topographic profiles (insets) after 3 MLs of Ga deposition on a GaAs surface for the following substrate temperatures: sample A annealed at 320°C , sample B at 490°C and sample C at 580°C . All AFM images are topographic.

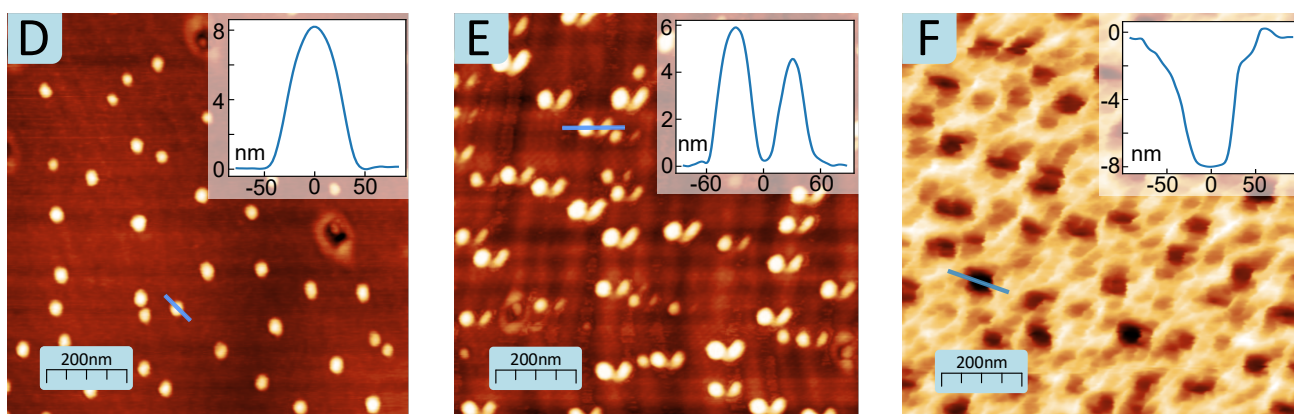


Figure 3. $1 \times 1 \mu\text{m}^2$ AFM images and topographic profiles (insets) of crystallised samples after 10 mins of As_4 irradiation at BEP 10^{-5} torr at the following substrate temperatures: sample D at 450°C , sample E at 520°C , sample F at 580°C . All AFM images are topographic.

350°C [17]. This suggests that other fabrication parameters shifts the dominant processes during this type of growth, such as exposing our samples to the atmosphere during splitting, and differences in initial droplet dimensions. The samples D to F demonstrate the extensive range of nanostructures obtained by varying only the crystallisation temperature during growth (Figure 4).

3.3. As_2 and As_4 Crystallisation Comparison

The AFM images in Figure 5 show the quantum structure morphology of samples G and H crystallised at 520°C with As_4 and As_2 respectively. Sample G contains QRs with diameter 40 ± 10 nm, height 1.5 ± 0.5 nm and density $(1.9 \pm 0.1) \times 10^{10} \text{cm}^{-2}$, whereas sample H achieved QRs with diameter 35 ± 5 nm, height 0.9 ± 0.1 nm and density $(3.7 \pm 0.1) \times 10^{10} \text{cm}^{-2}$. This shows a successful attempt to create QR's from a QD recipe with reduced BEP. By reducing the As BEP, liquid As becomes less available, reducing adsorption rate and allowing diffusion to

have more impact on the growth. The $\text{Al}_{0.32}\text{Ga}_{0.68}\text{As}$ surface does not encourage anisotropic diffusion. The nanorings developed following growth behaviour that has been observed in previous studies [25] and analysed theoretically [26, 17]. We suggest the high areal structural density as compared to samples A-F can be attributed to both the liquid material reaction with the $\text{Al}_{0.32}\text{Ga}_{0.68}\text{As}$ surface and the change in As BEP. The limited diameter and height of rings for sample H indicates that the Ga droplet has less time to diffuse at rate R_D before crystallising, which agrees with previous studies showing more efficient incorporation of As_2 than that of As_4 [27, 28]. This is further evidenced by the reduced QR density observed in sample G, as the Ga droplets have more time to nucleate together, due to a slower crystallisation and the growth pause required to tune the cracker temperature down for As_4 .

Using As_2 in the place of As_4 allows the fabrication of higher density structures with reduced diameters and height. This could be useful for higher

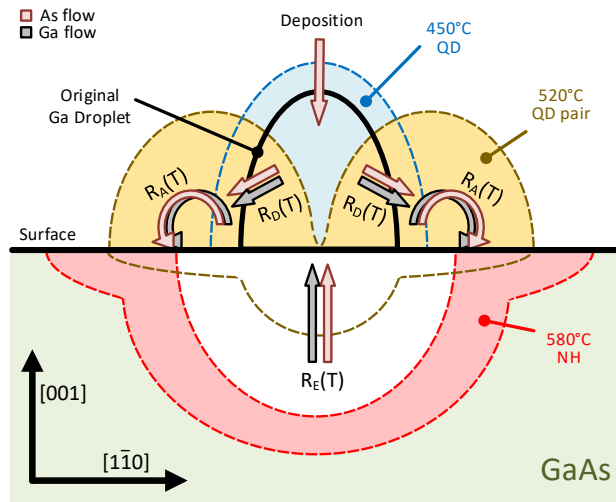


Figure 4. Schematic representation of various GaAs nanostructure topographical profiles formed experimentally from Ga droplets at various crystallisation temperatures (not to scale). Included are the evolution of Ga droplet into GaAs QDs at 450 °C (sample D), GaAs QD pairs at 520 °C (sample E) and GaAs nanoholes at 580 °C (sample F). The internal structure of the nanoholes (NH) has not been directly observed. R_D , R_E and R_A visualise the flow of diffusion, etching and adsorption rates respectively. R_D increases with temperature, which reduces nanostructure height. R_A is dominant at low temperature and allows crystallisation to occur before much diffusion takes place. R_E increases with higher temperature allowing the Ga droplet to drill into the substrate further.

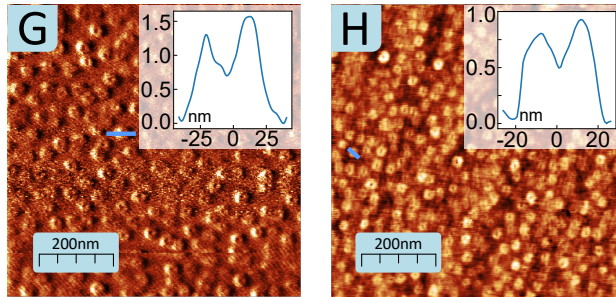


Figure 5. $1 \times 1 \mu\text{m}^2$ AFM scans showing As₄ crystallised GaAs/Al_{0.32}Ga_{0.68}As QRs (sample G) and As₂ crystallised GaAs/Al_{0.32}Ga_{0.68}As QRs (sample H). Both samples were crystallised at 520 °C and BEP 5×10^{-6} torr. For sample G, a tapping-mode AFM phase image is used instead of a topographic scan to highlight the intricacy of the ring shape. Both the insets show the topographic profiles of a nanostructure from the respective scans.

energy electron/hole confinement and reduced emission wavelength for optical applications. In addition, there is no growth pause required to tune the As₂ cracker temperature, which provides a more continuous growth procedure. The reduction of time between annealing and crystallisation limits Ga droplet nucleation and increases structure density, which can aid optical efficiency.

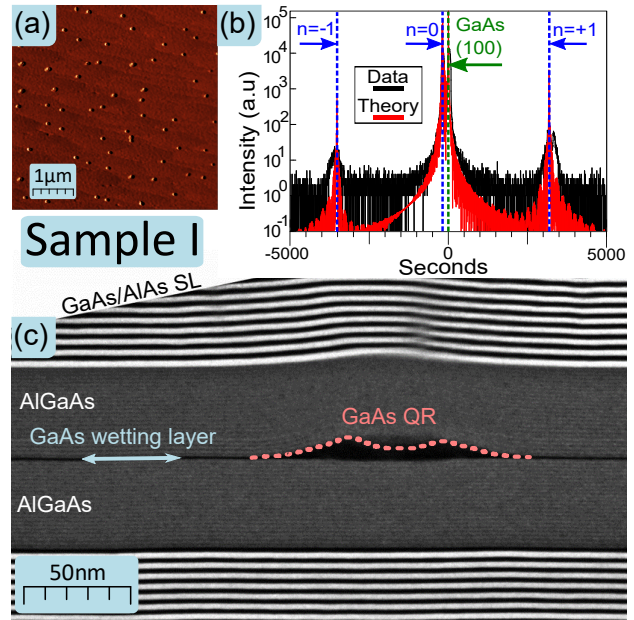


Figure 6. Measurements of sample I: (a) $5 \times 5 \mu\text{m}^2$ AFM scan showing As₂ crystallised GaAs/Al_{0.32}Ga_{0.68}As QRs (sample I). (b) X-ray diffraction of sample I centred on GaAs (100) reflection. The black line represents the measured intensity data, and the red line represents theoretical data generated from a model of the sample. (c) Cross-sectional bright-field TEM image of sample I showing the geometry of the SL structures, wetting layer and QR.

3.4. Structural and Optical Properties of QRs Embedded in a Superlattice

Figure 6(a) shows an AFM image of sample I's surface, the nanostructures have diameter 100 ± 10 nm, height 10 ± 1 nm and density $(3.0 \pm 0.1) \times 10^8 \text{ cm}^{-2}$. Figure 6(b) shows X-ray diffraction data of sample I centred on GaAs (001) reflection, along with simulated results. To the left of the centre, the first Bragg angle from the SL can be observed (labelled $n = 0$), the two peaks outward from the centre are the adjacent Bragg angles of the SL (labelled $n = \pm 1$), matching the theoretical model and suggesting a successful SL growth and correct Al/Ga ratio. The bright-field TEM image in Figure 6(c) shows a cross section of sample I, partially cutting through a GaAs QR embedded between Al_{0.32}Ga_{0.68}As layers and the SL. The QR has a diameter of ≈ 90 nm and a height of ≈ 10 nm. This is more than double the diameter of samples G and H, suggesting that the extra fabrication steps to build the sandwich layers has interfered with nanostructure growth. It also shows the presence of a 2 nm thick GaAs wetting layer (thin quantum well) below the GaAs QRs. This has materialised from an As-rich Al_{0.32}Ga_{0.68}As lower layer crystallising with the Ga deposited for creating droplets. The upper Al_{0.32}Ga_{0.68}As and SL have grown uniformly over the QR, producing a curvature in these layers.

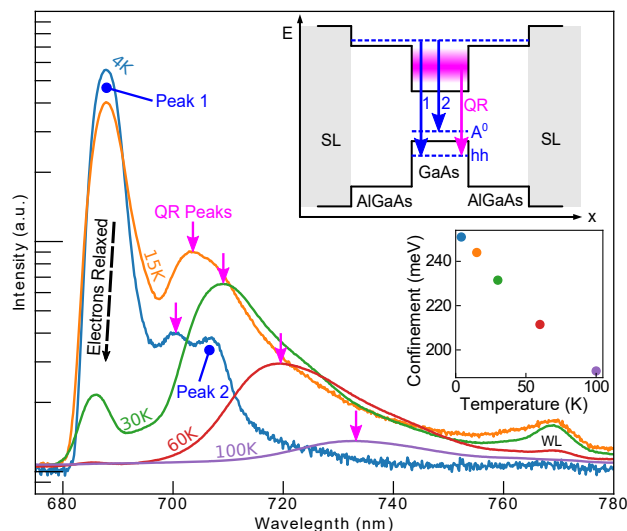


Figure 7. Log-scale photoluminescence (PL) intensity for sample I at a range of temperatures. The upper inset shows a schematic energy band diagram for the sample. At 4K the PL is dominated by recombination from electrons in the $\text{Al}_{0.32}\text{Ga}_{0.68}\text{As}$ layer to heavy holes (hh) in the GaAs QR (Peak 1). Electrons also recombine with an occupied carbon impurity acceptor state (A^0) in the GaAs QR (Peak 2). QR emissions between 700 nm and 780 nm become dominant at temperatures of 30 K and above (QR Peaks), however, individual energy states can not be distinguished due to thermal broadening. The accumulative QR emission maxima (pink arrows) have been fitted with Varshni's empirical expression to show their modal confinement energy in the lower inset, *i.e.* the difference between the PL energy observed and the GaAs bandgap. As the temperature increases, electrons relax into lower QR states and the emission maximum shifts to higher wavelength. A weak wetting layer signal (WL) is observed at 769 nm, across the temperature range.

Figure 7 shows PL measurements at temperatures from 4 K to 100 K, which contain a range of emission peaks. At 4 K, an intense peak at 689 nm (Peak 1) is observed from recombination of $\text{Al}_{0.32}\text{Ga}_{0.68}\text{As}$ layer electrons to heavy holes (hh) in the QR valence band [15]. Another peak (Peak 2) can be distinguished at 706 nm, which we attribute to recombination of electrons in the $\text{Al}_{0.32}\text{Ga}_{0.68}\text{As}$ with holes bound to a carbon impurity acceptor state (A^0) within the QR [15]. At 700 nm a signal is observed showing QR electron-hh recombination. At low temperature, electron access to pathways for relaxation is limited, suppressing transitions from GaAs QR states and causing peak 1 to be dominant. Peak 2 has low intensity, as it has been shown that it is associated with the presence of the phonon-bottleneck, which limits relaxation of electrons to A^0 [15]. As the temperature is raised above 4 K, an increase in available hh states lift the phonon bottleneck and suppress peak 2. More electrons can relax into the QR confined states, suppressing peak 1, and allowing a range of QR peaks between 700 nm and

740 nm to become dominant. The various unresolved QR peaks show the accumulative signals from the confined states of the GaAs QRs. Higher temperature combined with inhomogeneous broadening makes each peak indistinguishable. Focusing on the accumulative luminescence maxima, a modal QR quantum confinement of 190 – 250 meV at 100 – 4 K respectively is observed above the GaAs band gap as defined by Varshni's empirical expression [29]. The decreasing modal QR confinement with increasing temperature is caused by the lower confined states of the QRs becoming more easily accessed at higher temperature, when the carriers are thermalised and reach lower energy states before recombination [30]. PL emission from the wetting layer was observed at 768 nm, although this signal is weak compared to the QR emission.

4. Conclusion

We have investigated the evolution and topography of self-assembled GaAs quantum structures created with droplet epitaxy growth. In the interest of producing uniform, defect free Ga droplets, the optimal post-growth droplet annealing temperature was found to be 320 °C. During crystallisation under As_4 , the Ga and As surface atom diffusion, adsorption and etching processes can be controlled simply by adjusting the temperature of the sample. This single parameter can be chosen to create an extensive variety of complex GaAs nanostructures; quantum dots, quantum dot pairs and nanoholes. We find that surface adsorption is dominant at 450 °C, diffusion is activated at 520 °C, and etching is dominant at 580 °C. As_2 reacts and crystallises liquid Ga at a higher rate than As_4 , and therefore is observed to produce smaller nanostructures at higher density. Also, As_2 does not require a growth pause to adjust cracker temperature, therefore this material allows more efficient optical devices to be fabricated faster from the same materials. The realised low-density As_2 quantum rings within a superlattice demonstrate strong zero-dimensional carrier confinement resulting in PL emission from several transitions between 700 nm and 750 nm. These measurements imply that for droplet epitaxy, As_2 is equally capable as As_4 for creating high quality optoelectronic quantum structures and it removes the need to pause growth for tuning the cracker temperature. In particular, quantum rings in a superlattice created with As_2 have good potential for use as efficient photon emitters.

- [1] Kastner M A 1993 *AIP Conference Proceedings* **275** 573–586
- [2] Ledentsov N, Ustinov V, Shchukin V, Kop'ev P, Alferov Z I and Bimberg D 1998 *Semiconductors* **32** 343–365
- [3] Lent C S and Tougaw P D 1997 *Proceedings of the IEEE* **85** 541–557 ISSN 0018-9219

- [4] Lüth H 2001 *Interfaces and Thin Films. Springer* **4**
- [5] Smakman E, Garleff J, Young R, Hayne M, Rambabu P and Koenraad P 2012 *Applied Physics Letters* **100** 142116
- [6] Wu J, Shao D, Dorogan V G, Li A Z, Li S, DeCuir E A, Manasreh M O, Wang Z M, Mazur Y I and Salamo G J 2010 *Nano Letters* **10** 1512–1516
- [7] DeJarld M, Reyes K, Smereka P and Millunchick J 2013 *Applied Physics Letters* **102** 133107
- [8] Sablon K A, Lee J H, Wang Z M, Shultz J H and Salamo G J 2008 *Applied Physics Letters* **92** 203106
- [9] Alonso-González P, Alén B, Fuster D, González Y, González L and Martínez-Pastor J 2007 *Applied Physics Letters* **91** 163104
- [10] Somaschini C, Bietti S, Koguchi N and Sanguinetti S 2009 *Nano letters* **9** 3419–3424
- [11] Somaschini C, Bietti S, Scaccabarozzi A, Grilli E and Sanguinetti S 2012 *Crystal Growth & Design* **12** 1180–1184
- [12] Kunruga M, Panyakeow S and Ratanathammaphan S 2015 *Journal of Crystal Growth* **416** 73–77
- [13] Anyebe E, Zhuang Q, Sanchez A, Lawson S, Robson A, Ponomarenko L, Zhukov A and Kolosov O 2014 *physica status solidi (RRL) - Rapid Research Letters* **8** 658662 ISSN 1862-6254
- [14] Kuroda T, Mano T, Ha N, Nakajima H, Kumano H, Urbaszek B, Jo M, Abbarchi M, Sakuma Y, Sakoda K, Suemune I, Marie X and Amand T 2013 *Phys. Rev. B* **88**(4) 041306
- [15] Chang Y C, Robson A, Harrison S, Zhuang Q and Hayne M 2015 *AIP Advances* **5** 067141
- [16] Sidor Y, Partoens B, Peeters F M, Schildermans N, Hayne M, Moshchalkov V V, Rastelli A and Schmidt O G 2006 *Physical Review B* **73** 155334
- [17] Reyes K, Smereka P, Nothorn D, Millunchick J M, Bietti S, Somaschini C, Sanguinetti S and Frigeri C 2013 *Physical Review B* **87** 165406
- [18] Fomin V M 2018 Quantum ring: A unique playground for the quantum-mechanical paradigm *Physics of Quantum Rings* (Springer) pp 3–32
- [19] Vineyard G H 1957 *Journal of Physics and Chemistry of Solids* **3** 121 – 127 ISSN 0022-3697
- [20] Vasilenko M A, Neizvestny I G and Shwartz N L 2015 *Computational Materials Science* **102** 286–292
- [21] Kley A, Ruggerone P and Scheffler M 1997 *Physical review letters* **79** 5278
- [22] Wang Z M, Holmes K, Mazur Y I, Ramsey K A and Salamo G J 2006 *Nanoscale Research Letters* **1** 57 ISSN 1556-276X
- [23] Adorno S, Bietti S and Sanguinetti S 2013 *Journal of Crystal Growth* **378** 515–518
- [24] Li X, Wu J, Wang Z M, Liang B, Lee J, Kim E S and Salamo G J 2014 *Nanoscale* **6** 2675–2681
- [25] Somaschini C, Bietti S, Sanguinetti S, Koguchi N and Fedorov A 2010 *Nanotechnology* **21** 125601
- [26] Zhou Z Y, Zheng C X, Tang W X, Tersoff J and Jesson D E 2013 *Phys. Rev. Lett.* **111**(3) 036102
- [27] Garcia J, Neri C and Massies J 1989 *Journal of Crystal Growth* **98** 511 – 518 ISSN 0022-0248
- [28] Holmes D, Belk J, Sudijono J, Neave J, Jones T and Joyce B 1995 *Applied physics letters* **67** 2848–2850
- [29] Varshni Y P 1967 *physica* **34** 149–154
- [30] Nuytten T, Hayne M, Bansal B, Liu H, Hopkinson M and Moshchalkov V V 2011 *Physical Review B* **84** 045302